CrystEngComm

Accepted Manuscript

This is an *Accepted Manuscript*, which has been through the Royal Society of Chemistry peer review process and has been accepted for publication.

Accepted Manuscripts are published online shortly after acceptance, before technical editing, formatting and proof reading. Using this free service, authors can make their results available to the community, in citable form, before we publish the edited article. We will replace this *Accepted Manuscript* with the edited and formatted *Advance Article* as soon as it is available.

You can find more information about *Accepted Manuscripts* in the Information for Authors.

Please note that technical editing may introduce minor changes to the text and/or graphics, which may alter content. The journal's standard Terms & Conditions and the Ethical guidelines still apply. In no event shall the Royal Society of Chemistry be held responsible for any errors or omissions in this *Accepted Manuscript* or any consequences arising from the use of any information it contains.

ROYAL SOCIETY OF CHEMISTRY

www.rsc.org/crystengcomm

Please do not adjust margins

CrystEngComm

ARTICLE

Modification of crystal structure of $Sr_{2-x}Ba_xSi(O,N)_4$: Eu^{2+} phosphors to improve luminescence properties

Received 00th January 20xx,
Accepted 00th January 20xx

DOI: 10.1039/x0xx00000x

www.rsc.org/

Xiaojun Li,[a] Youjie Hua,*[a] Hongping Ma,[b] Degang Deng[a] and Shiqing Xu*[a]

Abstract: A series of $Sr_{1.98-x}Ba_xSi(O,N)_4$: $0.02Eu^{2+}$ ($0 \le x \le 0.5$) phosphors were synthesized by conventional solid state reaction method. The Sr-N and Si-N bond could be observed in FT-IR spectra. The XRD refinement results indicated that N^{3-} would substitute for $O2^{2-}$ site and form Si-NO3 tetrahedrons during the process of forming $Sr_{1.98}Si(O,N)_4$: Eu^{2+} (SSON : Eu^{2+}) substitutional solid solution. The lattice constants of $Sr_{1.98-x}Ba_xSi(O,N)_4$: $0.02Eu^{2+}$ (SBSON) were expanded due to the longer bond length of Ba–O. Compared with Sr_2SiO_4: Eu^{2+}, the SSON: Eu^{2+} showed a remarkable red-shift, which is due to the nephelauxetic effect and the strong crystal field splitting originated from stronger covalent bonding effect of Eu-N bond. The SSON: Eu^{2+} present β phase structure before the introduction of Ba^{2+}, whereas the α'-SBSON phase was obtained by the substitution of Ba^{2+} for Sr^{2+}. Ba^{2+} doping led to an obvious blue-shift under 375 nm and 460 nm excitation. The 5d orbital of Ba^{2+} coupled with the 5d orbital of Eu^{2+} on the higher energy level position in the host crystal. Under 375 nm excitation, the PL intensity gradually increased with the increase of Ba^{2+} content. Under 460 nm excitation, the PL intensity gradually declined with the increase of Ba^{2+} content. The thermostability of α'-SBSON: Eu^{2+} was significantly improved compared with β-SSO: Eu^{2+} and β-SSON: Eu^{2+}. On the base of the adjustable emission wavelength, enhanced PL intensity and excellent thermostability in SBSON: Eu^{2+}, we anticipate that these materials can be used as green or red phosphor in white light emitting diodes.

1 Introduction

Recently, a new package type that combined with color-tunable phosphors and n-UV or blue chips has been developed rapidly. As a series of important silicate materials, the RE-doped M_2SiO_4 (M=Ca, Sr, Ba, Mg) phosphors can easily achieved colour tuning through the chemical composition and structural modification. Such as the $Sr_xBa_{2-x}SiO_4$: Eu^{2+} and $Ca_{1-y}Sr_{1-y}Si_{1-x}Al_xO_4$: yCe^{3+}, yLi^+ phosphors with enhanced luminescence properties by doped ions;[1,2] the white emitting phosphors of single materials $(Ba,Ca)_2SiO_4$: Eu^{2+}, Mn^{2+} and Li_2SrSiO_4: Eu^{2+},Ce^{3+};[3-5] and the green phosphors $Ca_{1.65}Sr_{0.35}SiO_4$: Ce^{3+},Li^+,Eu^{2+} and $BaMgSiO_4$: Eu^{2+}.[6-7] These studies suggest that the colour and crystal structure tunable RE-doped M_2SiO_4 (M=Ca, Sr, Ba, Mg) phosphors have enormous potential for the application of phosphor-converted white light emitting diodes (pc-LEDs).

The Sr_2SiO_4: Eu^{2+} phosphors have been extensively studied due to their special structural features and potential applications in developing white light-emitting-diodes.[8-11] The orthosilicate phosphor of Sr_2SiO_4: Eu^{2+} has two crystallographic phases: high temperature α'–Sr_2SiO_4 (orthorhombic) phase and low temperature β–Sr_2SiO_4 (monoclinic) phase.[12-14] Both the α' and β phase have two luminescence center: Eu(I) and Eu(II). Eu(I) is ten-coordinated and Eu(II) is nine-coordinated by oxygen atoms within a limited range.[15-17] Recently, due to the remarkable emission in the red wavelength, the Sr_2SiO_4: Eu^{2+} with N^{3-} substitution (SSON: Eu^{2+}) has been reported in some literatures.[18-23] These research mainly included the following five aspects: (a) the detailed crystal structure;[19] (b) the replacement of M^{2+} cations (M= Ca, Ba, Mg);[20] (c) the distinction from Eu(I) and Eu(II) due to nitridation;[21] (d) the detail of coordination environment of Eu^{2+} and the interaction mechanism of nitrogen on red-shift emission.[22] (e) the effects of N^{3-} ions on the crystal structure and luminescent properties of α'-$Sr_2Si_{3x/4}O_2N_x$: Eu^{2+} ($1.333 \le x \le 2.4$) by varying N content.[23] However, the phase transformation of SSON: Eu^{2+} and the change of PL intensity with varying substitution content of cations have not been effectively researched. It is necessary to control the phase compositions of the SSON: Eu^{2+} phosphors and study the change of crystal structure and photoluminescence properties depending on the substitution of N^{3-} and Ba^{2+}.

In the case of Sr_2SiO_4, the β (monoclinic) ↔ α' (orthorhombic) phase transformation occurs at 358K.[12] The phase transformation occurs through a short-range rearrangement of the coordination structure without breaking coordination bonds (displacive transformation).[12, 24] High calcination temperature promoted the phase transformation from α'–Sr_2SiO_4 (orthorhombic) to β–Sr_2SiO_4 (monoclinic), while the doping of Eu or Ba ions could stabilize α'–Sr_2SiO_4 phase due to their long bond length with oxygen.[10,25]

In this paper, the $Sr_{1.98-x}Ba_xSi(O,N)_4$: $0.02Eu^{2+}$ ($0 \le x \le 0.5$) phosphors were successfully synthesized by the conventional solid-state reaction method. We investigated the effects of Ba^{2+} substitution on the crystal structural and luminescence properties

[a] College of Materials Science and Engineering, China Jiliang University, Hangzhou 310018, China. Fax: +86-571-28889527; Tel: +86-571-86835781; E-mail: sxucjlu@163.com
[b] School of Mechanical & Automotive Engineering, Zhejiang University of Science and Technology, Hangzhou 310012, China

CrystEngComm Accepted Manuscript

of α′-SSON: Eu^{2+} by varying Ba^{2+} content. The Sr-N and Si-N bond were confirmed by crystal structure and FI-IR spectra and the specific site of N substituting for O was determined. The specific reasons of PL intensity change and phase transformation were explained. The crystal of SSON: Eu^{2+} could be effectively controlled by Ba^{2+} doping and could achieve higher PL intensity of SSON: Eu^{2+} based on modification of the crystal structure.

2 Experimental

2.1 Sample preparation

The $Sr_{1.98-x}Ba_xSi(O,N)_4$: $0.02Eu^{2+}$ ($0 \le x \le 0.5$) was prepared by solid state reactions in a horizontal tube furnace using starting materials of $SrCO_3$ (AR), $BaCO_3$ (AR), α-Si_3N_4 (Alfa 99.9%), SiO_2 (AR) and Eu_2O_3(99.9%).

All the raw materials were mixed in an agate mortar and then filled into BN crucibles. The powder mixtures were preheated at 1050 ℃ for 2 h, and then fired at 1450℃ (with a heating rate of 5℃ /min) for 7h, followed by cooling down to 300 ℃ at a rate of 5 ℃ /min and down to room temperature spontaneously in the furnace with the power switched off. In order to prevent samples from being oxidized, all heating and cooling processes were conducted in a flowing reductive atmosphere of 5:95 (volume) H_2/N_2.

2.2 Characterization

The phase composition and crystallinity of the synthesized samples were investigated by powder X-ray diffraction (BrukerAxs D2 PHASER diffractometer) with Cu Kα radiation (λ= 1.5405 Å) over the angular range $10° \le 2\theta \le 80°$, operating at 30 kV and 10 mA. The excitation and emission spectra of the phosphors were measured at room temperature on a PL3-211-P spectrometer (HORIBA JOBIN YVON, America) and a 450W xenon lamp was used as the excitation source. The PL decay-curves were measured on the same spectrometer, which was combined with a Time-Correlated Single-Photon Counting (TCSPC) system. The crystallographic data including lattice parameters, unit cell volume, and phase ratios were estimated by the TOPAS package based on the XRD data, using the Sr_2SiO_4 structure as a starting model. The nitrogen and oxygen contents (Atomic %) were measured by energy dispersive spectrometry system (TEAM Apollo XL EDS, EDAX, America). Fourier-transform infrared spectra (FT-IR) were measured on a BRUKER TENSOR 27 spectrophotometer in the range of 400–4000 cm^{-1} using the KBr pellet (~2wt %) method. The absorbance spectra of the samples were measured by an ultraviolet-visible-near infrared spectrophotometer (Uv3600) using BaSO4 as a reference in the range of 200–800 nm. All the above measurements were performed at room temperature.

3 Results and discussion,

3.1 X-ray diffraction analysis and crystal structure

Fig. 1 (a) shows the XRD patterns of β-$Sr_{1.98}SiO_4$: $0.02Eu^{2+}$ and $Sr_{1.98-x}Ba_xSi(O,N)_4$: $0.02Eu^{2+}$ ($0 \le x \le 0.5$) with different x values. As shown in Fig. 1, the $Sr_{1.98}Si(O,N)_4$: $0.02Eu^{2+}$ (x=0, SSON: $0.02Eu^{2+}$) matched well with the β-Sr_2SiO_4 (β-SSO, JCPDS no.38-0271) phase. In comparison with the β-Sr_2SiO_4, the degree of crystallinity of β-SSON became worse. However, with the increase of x value from 0.1 to 0.5, all the samples of the $Sr_{1.98-x}Ba_xSi(O,N)_4$: $0.02Eu^{2+}$ ($0.1 \le x \le 0.5$, SBSON: $0.02Eu^{2+}$) matched well with the α′-Sr_2SiO_4 (α′-SSO, JCPDS no.39-1256) phase. All the α′-SBSON phases have similar XRD patterns because α′-$Sr_{1.9}Ba_{0.1}SiO_4$ had the same structure with α′-Sr_2SiO_4 where divalent Ba^{2+} ions occupy the sites of Sr^{2+}.[8, 12] The degree of crystallinity of α′-SBSON gradually decreased with the increase of Ba content. Besides, there were no Ba_2SiO_4 phases in SBSON when the Ba^{2+} ions substation content increased from 0.1 to 0.5. These results indicate that the β-SSON transformed from β to α′ phase because Ba^{2+} ions substituted for Sr^{2+} ions. Fig. 1 (b) shows the local amplificatory XRD patterns of SBSON: $0.02Eu^{2+}$ in the range of 26.25°-32°. As shown in Fig. 1 (b), Ba^{2+} doping led to the results that XRD diffraction peaks shifted in the direction of smaller angle. This is because Ba^{2+} doping led to the lattice expansion of the α′ phase depending on the larger ionic radius of Ba^{2+} (1.49 Å for 9CN, 1.52 Å for 10CN) than that of Sr^{2+} (1.30 Å for 9CN, 1.35 Å for 10CN).

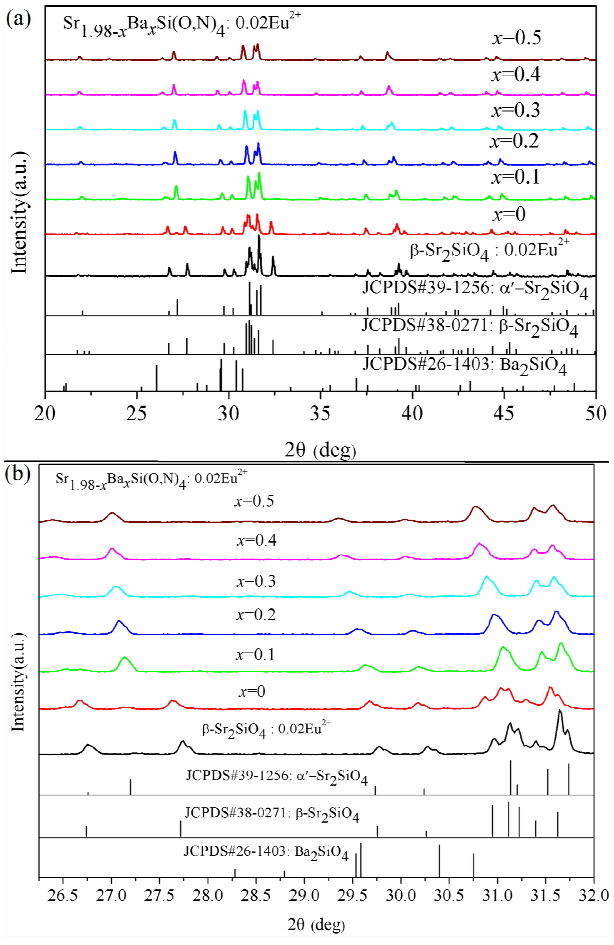

Fig. 1 XRD patterns of $Sr_{1.98-x}Ba_xSi(O,N)_4$: $0.02Eu^{2+}$ ($0 \le x \le 0.5$) with various Ba^{2+} content and β-Sr_2SiO_4: $0.02Eu^{2+}$.

CrystEngComm Accepted Manuscript

This journal is © The Royal Society of Chemistry 20xx

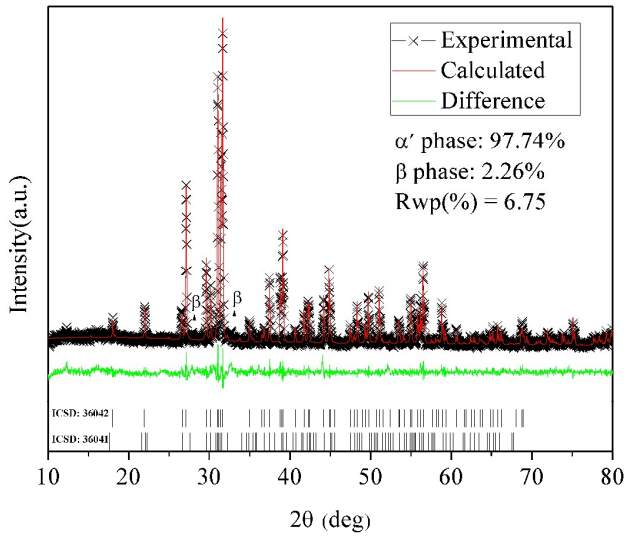

Fig. 2 Rietveld refinement XRD patterns of α′- $Sr_{1.9}Ba_{0.1}Si(O,N)_4$: $0.02Eu^{2+}$ by TOPAS package. (Observed– black line, calculated– red line and difference– green line).

The crystal structure of α′-$Sr_{1.9}Ba_{0.1}Si(O,N)_4$: $0.02Eu^{2+}$ was analyzed by TOPAS package on the basis of the XRD data, using the α′-Sr_2SiO_4 (ICSD: 35667), β-Sr_2SiO_4 (ICSD: 36041) structure as starting models. Fig. 2 shows the observed (black line), calculated (red line) and difference (green line) XRD profiles for the XRD Rietveld refinement of α′-$Sr_{1.9}Ba_{0.1}Si(O,N)_4$: $0.02Eu^{2+}$. The peaks (2θ=27.83° and 32.81°) of β phase was marked as β symbol in Fig. 2. These results indicate that a predominant pure α′-SBSON phase have been formed accompanied by a small portion (2.26%) of β phase.

Table 1 lists the XRD refinement data of the α′- $Sr_{1.9}Ba_{0.1}Si(O,N)_4$: $0.02Eu^{2+}$. These refinement data include crystallographic parameters, reliability factors, wyckoff site, atomic coordinates, occupancy, and beq. The α′-$Sr_{1.9}Ba_{0.1}Si(O,N)_4$ crystallizes in an orthorhombic unit cell belonging to a space group of *Pmnb*: *ba-c* (no. 62). The refinement finally converged to R_{exp}= 5.08, R_{wp}=6.37, R_p=4.99 and GOF =1.25, as shown in Table 2. There are obvious differences of the atomic positions and cell volume between the α′-$Sr_{1.9}Ba_{0.1}SiO_4$: Eu^{2+} (391.81 Å^3) and α′-$Sr_{1.9}Ba_{0.1}Si(O,N)_4$: Eu^{2+} (395.8783 Å^3) according to ref. 8 and 12.

Table 1 Rietveld refinement and crystal data for α′- $Sr_{1.9}Ba_{0.1}Si(O,N)_4$

Space group: *Pmnb*: *ba-c* (orthorhombic)

Cell parameter	Reliability factors
a= 5.6796452Å	R_{exp}(%) = 5.10
b=7.1386574Å	R_{wp}（%）=6.75
c= 9.7639138Å	R_p（%）=5.28
Cell Volume = 395.87829 Å^3	Goodness of fit =1.32
Radiation (Å): Cu-Kα (λ = 1.54056 Å)	Density: 8.434g/cm^3
T=300K	z=4

Site	Np	x	y	z	Atom	Occ	Beq
Sr1	4c	0.24994	0.34014	0.58431	Sr^{+2}	0.95	0.6832
Ba1	4c	0.24994	0.34014	0.58431	Ba^{+2}	0.05	0.6832
Sr2	4c	0.23628	0.00114	0.30213	Sr^{+2}	0.95	1.913
Ba2	4c	0.23628	0.00114	0.30213	Ba^{+2}	0.05	1.913
Si1	4c	0.26068	0.78860	0.59495	Si^{+4}	0.5	1.714
O1	4c	0.31312	0.99852	0.56233	O^{-2}	0.5	1.494
N1	4c	0.27104	0.68820	0.43588	N^{-3}	0.5	3.186
O2	8d	0.47287	0.47287	0.65649	O^{-2}	1	-7.837

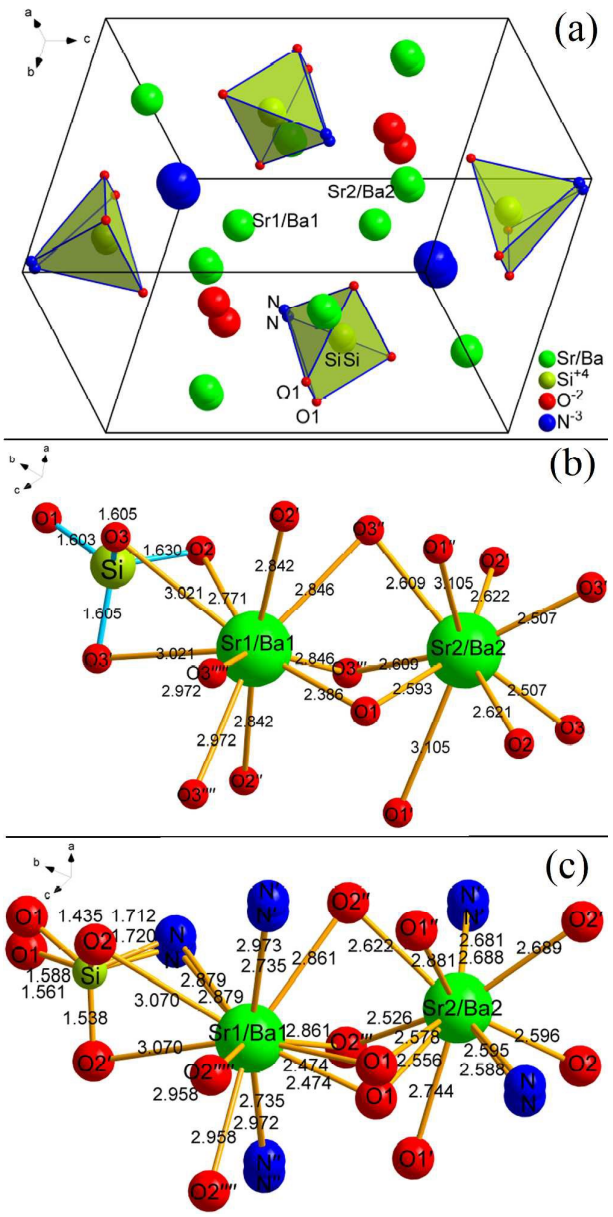

Fig. 3 (a) A unit cell of the α′-$Sr_{1.9}Ba_{0.1}Si(O,N)_4$: Eu^{2+} view in the [101] direction along b axis; (b) Coordination spheres of the Si and two different Sr^{2+}/Ba^{2+} sites of the ICSD-36042: ordered α′-$Sr_{1.9}Ba_{0.1}SiO_4$; (c) Coordination spheres of the Si and two different Sr^{2+}/Ba^{2+} sites of the α′-$Sr_{1.9}Ba_{0.1}Si(O,N)_4$.

CrystEngComm Accepted Manuscript

Fig. 3 (a) shows a unit cell of the α′-$Sr_{1.9}Ba_{0.1}Si(O,N)_4:Eu^{2+}$ view toward the [111] plane. The Si (N/O) 4 tetrahedra and Sr/Ba polyhedra showed a hexagonal pseudo-symmetry along [101] in the single unit cell, as was confirmed by the c/a ratio which was close to $\sqrt{3}$. The structural type is characterized by [010] chains of Sr coordination polyhedral sharing faces, which are linked with one another forming a three-dimensional framework of polyhedra.[12] Fig. 3 (b) shows the coordination spheres of the Si and two different Sr^{2+}/Ba^{2+} sites of the α′-$Sr_{1.9}Ba_{0.1}SiO_4$, which is obtained by ISCD-36042. Fig. 3 (c) shows coordination spheres of the Si and two different Sr^{2+}/Ba^{2+} sites of the α′- $Sr_{1.9}Ba_{0.1}Si(O,N)_4$, which is obtained by Rietveld refinement data in Table 1.

Due to the change of O atoms positions and occupation, the α′-Sr_2SiO_4 phase has two structure models: disordered (isotropic) and ordered (anisotropic) model.[13] However, the mixed-model in α′-Sr_2SiO_4 as follow: The O1 and O2 atoms lying on the mirror plane (x ≈ 0.25) was split into two, in very close positions equivalent by m symmetry, with 0.5 occupation factor (o.f.) and refined isotropically (disordered). The O1', O2' were out of the mirror plane (x ≠ 0.25, o.f. = p) and O1", O2" were in the mirror plane (x = 0.25, o.f. = 0.5-p). The o.f.'s of O3 and O4 were constrained to be 1-p and p, respectively. The p parameter was ranging from 0 (pure order phase) to 0.5 (pure disorder phase). As shown in Fig. 3 (a) and (c), in our experiments, the results of refinement indicate that α′-$Sr_{1.9}Ba_{0.1}Si(O,N)_4$ presents mixed ordered (p=0) and disordered (the symmetric splitting sites of Si, O1 and N atoms) phase feature. However, the ordered α′-SBSON phase was dominant because the disordered α′ phase has four different O atoms sites.[13] In addition, Fig. 3 (b) and (c) indicated that the Sr/Ba^{2+} ions in α′-SBSO and α′-SBSON have two sites: (Sr/Ba)1 and (Sr/Ba)2. (Sr/Ba)1 is 10-fold coordinated (CN=10) whereas (Sr/Ba)2 is 9-fold coordinated (CN =9) by oxygen atoms within a limited range.

The bond length of Si-O2 increased from 1.630 Å to ~1.72 Å after N^{3-} substituting for O^{2-}. The observed Si–N bonds in other silicon-based oxynitrides were in the range of 1.660~1.750 Å, as shown in Table 2. Therefore, it could be speculated that the N^{3-} would substitute for $O2^{2-}$ site during the process of formation of α′-SBSON solid-solution, as shown in Fig. 3 (c). However, paradoxically, the Si-O1, Si-O3 and Si-O3′ bond lengths in α′-$Sr_{1.9}Ba_{0.1}Si(O,N)_4$ deviated from the normal ranges observed in other silicon-based oxynitrides and got shorter than ordered α′-$Sr_{1.9}Ba_{0.1}SiO_4$, as shown in Table 2. Thus the Si-O1, Si-O3, Si-O3′ and Si-N in α′-SBSON formed Si-NO_3 tetrahedrons. The α′-$Sr_{1.9}Ba_{0.1}Si(O,N)_4$ is a substitutional solid solution due to the substitutions of N^{3-} and Ba^{2+} ions. During the process of forming Si-NO_3 tetrahedrons in substitutional solid solution α′-SBSON, the Si-O bonds were squeezed by the longer Si-N bonds due to the covalent bond effect.[23, 26] Hence, the Si-O1, Si-O3 and Si-O3′ bonds got shorter obviously after N^{3-} substituting for $O2^{2-}$ site. The other silicon-based oxynitrides didn't appeared obvious squeeze effect because they are not solid-solutions. Thus the Si-O bond lengths of other silicon-based oxynitrides are within the normal ranges. These results demonstrate that N^{3-} ions have partially been incorporated into the α′-SBSO lattice, forming a solid-solution of α′-SBSON.

Table 2 The Si-(N/O) bond lengths with different tetrahedrons types

Silicon-based oxynitrides	Tetrahedron types	Si–O bond lengths (Å)	Si–N bond lengths (Å)
$Y_4Si_2O_7N_2$ (ref. 27)	Si-NO_3	1.595–1.706	1.708, 1.731
$Sr_3Si_2O_4N_2$ (ref. 28)	Si-N_2O_2	1.619–1.657	1.660–1.732
$SrSi_2O_2N_2$ (ref. 29)	Si-N_3O	1.603–1.608	1.740–1.746
ordered α′-SBSO	Si-O_4	1.603-1.630	
α′-SBSON	Si-$(N/O)_4$	1.458–1.558	1.800

Fig. 4 shows the bond length change of Sr1/Ba1-O and Sr2/Ba2-O bonds in the ordered α′-$Sr_{1.9}Ba_{0.1}SiO_4$ and α′-$Sr_{1.9}Ba_{0.1}Si(O,N)_4$. All the bond length values were obtained from Fig. 3. To be convenient for comparison, the N and O2 in SBSON was set as O2 and O3 respectively, which was consistent with the ordered α′-$Sr_{1.9}Ba_{0.1}SiO_4$. As shown in Fig. 4, compared with the other (Sr, Ba)-O bond length, the (Sr, Ba)1-O2 and part of (Sr, Ba)2-O3 (O3 and O3′) bond length of α′-SBSON got longer than that of ordered α′-SBSO. Besides, the variation of (Sr, Ba)1-O2 bond was more obvious than that of (Sr, Ba)2-O3 bond. On the other hand, the larger ionic radius will lead to longer ionic bond length because the ionic bond length is the sum of anion and cation radius. The ionic radius of N^{3-} (1.32 Å) is larger than that of O^{2-} (1.24 Å). So theoretically, the N^{3-} substitution for O^{2-} could make the bond length of Sr–O get longer. However, the Sr2-O1 bond length of SBSON got shorter obviously than that of SBSO, which should be ascribed to squeeze effect. It would lead to different spectra variation between the Eu(I) and Eu(II) sites. The results of our experiment are consistent with the theoretical analysis. Therefore, we can speculate that N^{3-} was easier to substitute for the O2 site than O3 and O1 site, which was consistent with the Si-O/N bond length analysis of Si-NO_3 tetrahedrons as shown in Fig. 3.

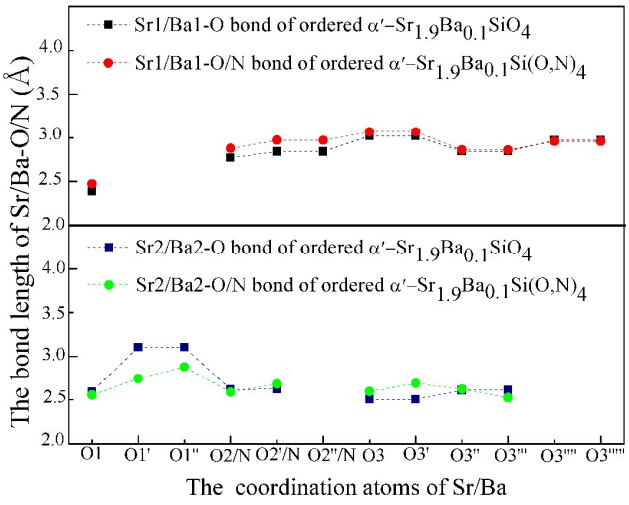

Fig. 4 The bond length contrast patterns of Sr1/Sr2-O between the α′-$Sr_{1.9}Ba_{0.1}SiO_4$ and α′-$Sr_{1.9}Ba_{0.1}Si(O,N)_4$.

Table 3 shows the results of XRD Rietveld refinement data of $Sr_{1.98-x}Ba_xSi(O,N)_4$: $0.02Eu^{2+}$ ($0 \le x \le 0.5$) with various Ba content. As shown in Table 3, the phase transformation of SSON from β to α′ phase obviously occurred when 0.1 mol Ba^{2+} ions entered into the

CrystEngComm Accepted Manuscript

This journal is © The Royal Society of Chemistry 20xx

crystal lattice. With the Ba content increasing from 0.1 to 0.5, the α′ phase was the major phase and the unit cell volume gradually increased. The XRD Rietveld refinement results showed that a small amount of Eu^{2+} and Ba^{2+} ions could enter into the host lattice of α′-SSON without destroying the crystal structure. In fact, Ba^{2+} had been reported as a stabilizer with the function of stabilizing metastable phase due to its larger ionic radius (0.152 nm).[25] It is known that the high-temperature α′-Sr_2SiO_4 phase can be stabilized at room temperature by substituting Ba^{2+} for Sr^{2+}.[8, 12] The formation of α′-SBSON phase phosphors (Fig. 1) could confirm the stabilizing effect of Ba^{2+} on the crystalline structure of α′-SSON: Eu^{2+}. The α′ ↔ β transition of Sr_2SiO_4 (SSO) can be simply accomplished by a rearrangement of atoms without breaking coordination bonds (displacive transformation).[13, 25] When a proper amount of Ba^{2+} was entered into SSON, similar to SSO, the displacive transformation from β-SSON to α′-SSON phase occurred, as shown in Fig.1 and Table 3.

Table 3 Lattice parameters of $Sr_{1.98-x}Ba_xSi(O,N)_4$: $0.02Eu^{2+}$ ($0 \le x \le 0.5$) (unit: Å, degree)

x	a	b	c	β	V (Å^3)	Rwp	α′-SSON
0(β)	5.6614	7.0847	9.7566	92.59	390.93	6.85	1.57%
0.1	5.6796	7.1386	9.7639	90	395.88	6.75	97.74%
0.2	5.6743	7.1136	9.7542	90	397.73	6.73	96.95%
0.3.	5.6802	7.1391	9.7646	90	399.97	6.68	96.98%
0.4	5.6858	7.1658	9.7734	90	401.20	6.64	97.46%
0.5	5.6903	7.1874	9.7844	90	403.16	7.38	97.27%
α′-SSO	5.682	7.090	9.773	90	393.71		
β-SSO	5.663	7.084	9.767	92.67	391.39		

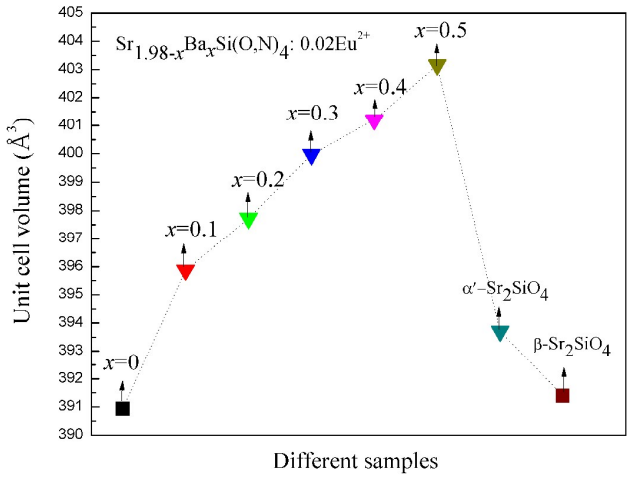

Fig. 5 Unit cell volume of SBSON: $0.02Eu^{2+}$ ($0 \le x \le 0.5$), α′-Sr_2SiO_4 and β-Sr_2SiO_4

Fig. 5 indicates the unit cell volume of SBSON: $0.02Eu^{2+}$ ($0 \le x \le 0.5$), α′-SSO and β-SSO. The unit cell volume gradually increased with the increase of the doped Ba^{2+} content. The ionic radius of Ba^{2+} (1.49 Å for 9CN, 1.52 Å for 10CN) is larger than that of Sr^{2+} (1.30 Å for 9CN, 1.35 Å for 10CN) and the ionic bond length is the sum of anion and cation radius. So the bond length of Ba-O is longer than that of Sr-O. Therefore, the expansion of the lattice constants with increasing Ba-content should be ascribed to the longer bond length of Ba-O than that of Sr-O.

3.2 N/O contents for $Sr_{1.98-x}Ba_xSi(O,N)_4$: $0.02Eu^{2+}$ ($0 \le x \le 0.5$) as a function of *x*

The N/O contents were measured by energy dispersive spectrometry system (EDS). Table 4 shows the experimental and theoretical calculation values of N/O contents. With the increase of *x* from 0 to 0.5, the experimental and the theoretical values of N/O contents in SSON or SBSON had a little difference due to the surface oxidation and the measuring error. When the introduction of Ba^{2+} ions increased from 0 to 0.1, the nitrogen content increased from 13.70 % to 15.67 % obviously. With the further introduction of Ba^{2+} ions, the nitrogen content hardly changed. This can be ascribed to the stabilization effect of Ba^{2+} in metastable phase.[25]

Table 4. The measured oxygen and nitrogen content in $Sr_{1.98-x}Ba_xSi(O,N)_4$: $0.02Eu^{2+}$ ($0 \le x \le 0.5$)

Sample	Nitrogen (Atomic %	Oxygen (Atomic	Theoretical value of the N contents (Atomic %)
SSON(*x*=0)	13.70	31.87	21.05
SBSON(*x*=0.1)	15.67	31.83	21.05
SBSON(*x*=0.2)	15.55	32.34	21.05
SBSON(*x*=0.3)	15.09	31.77	21.05
SBSON(*x*=0.4)	15.48	31.34	21.05
SBSON(*x*=0..5)	15.63	31.90	21.05

3.3 Comparison of FT-IR spectra for α′-SSO: Eu^{2+}, α′-SBSON: Eu^{2+}, β-SSO: Eu^{2+}, and β-SSON: Eu^{2+}.

Fig. 6 presents the FT-IR spectra of α′-SSO: Eu^{2+}, α′-SBSON: Eu^{2+}, β-SSO: Eu^{2+}, β-SSON: Eu^{2+} and $Sr_2Si_5N_8$: Eu^{2+} phosphors. Apparently, these FT-IR spectra show remarkable differences among these phosphors. The peak of 1475 cm^{-1} was assigned to Sr/Eu–O bond of α′ phase,[22] whereas the peak of 1636 cm^{-1} was assigned to Sr/Eu–O bond of β phase. This was because the monoclinic β phase (α=γ=90°, β=92.67°) have higher energy than the orthorhombic α′ phase (α=β=γ=90°).[12, 13] The longer bond length would lead to the weaker bond energy. Thus the absorption energy of Sr/Eu–N bond was lower than that of Sr/Eu–O bond due to the longer bond length of Sr-N than that of Sr-O. As shown in Fig, 6, the α′-SBSON: Eu^{2+} contained a new peak of 1364 cm^{-1} which was assigned to Sr/Eu–N bond,[22, 23] while the α′-SSO didn't show such peak. The β-SSON: Eu^{2+} contained a new peak of 1439 cm^{-1} which was also assigned to Sr/Eu–N bond, while the β-SSO didn't show such peak. Besides, the vibration energy of Sr/Eu–N bond in α′-SBSON (1364 cm^{-1}) and β-SSON: Eu^{2+} (1439 cm^{-1}) were different from the Sr/Eu–N bond in $Sr_2Si_5N_8$ (1633 cm^{-1}).

As show in the shaded area of Fig. 6, the absorption bands of Si-

CrystEngComm Accepted Manuscript

$(N/O)_4$ tetrahedrons with symmetric and antisymmetric stretching vibration were in the range of vibration energy (700 cm^{-1}-1100 cm^{-1}).[30-32] The larger the distinction of Si-O/N bond energy, the borader the absorption band of Si-$(N/O)_4$ tetrahedrons. The longer bond length would lead to the weaker bond energy. The distinction of Si-O bond length in α'-SSO was larger than β-SSO.[12, 13] Thus the Si-O_4 absorption band of α'-SSO was borader than that of β-SSO. The quantity of Si-N bond increased simultaneously along with the intrduction of N^{3-}. The bond energy of Si-N was lower than Si-O due to the longer bond length of Si-N than that of Si-O. Therefore, the Si-O_4 absorption was boraded and became Si-$(N/O)_4$ absorption band during the process of formation of α'-SBSON and β'-SSON solid-solutions, as shown in the shaded area of Fig. 6. Besides, the Si-N_4 absorption band of $Sr_2Si_5N_8$ was narrower than the Si-$(N/O)_4$ absorption of SSON due to the smaller distinction among the Si-N_4 bond energy. These results also confirm that nitrogen had entered the crystal lattice and formed chemical bonds with surrounding Sr^{2+}/Eu^{2+} ions and Si atoms in the α'-SBSON: Eu^{2+} and β-SSON phosphors.

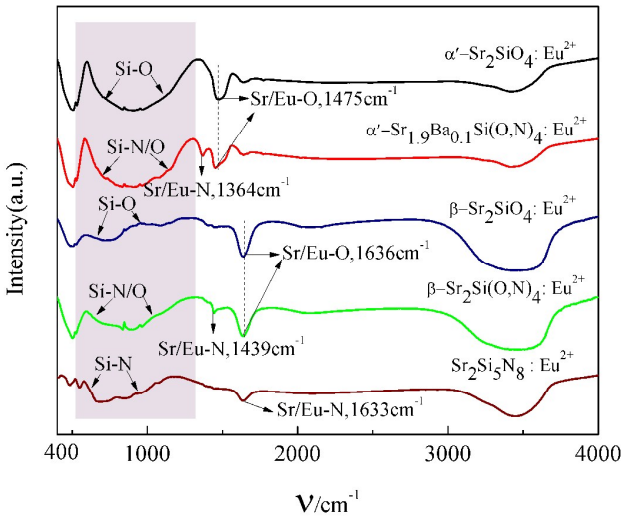

Fig. 6 FT-IR spectra of α'-SSO: Eu^{2+}, α'-SBSON: Eu^{2+}, β-SSO: Eu^{2+}, β-SSON: Eu^{2+} and $Sr_2Si_5N_8$: Eu^{2+} phosphors.

3.4 Luminescence properties of $Sr_{1.98-x}Ba_xSi(O,N)_4$: 0.02Eu^{2+} ($0 \le x \le 0.5$)

Fig. 7 shows the photoluminescence (PL) spectra of β-SSO: Eu^{2+} and β-SSON: Eu^{2+} under 375 nm and 460 nm excitation and the corresponding photoluminescence excitation (PLE) spectra. The dominant peak wavelengths (DPWs) of the Eu(I) and Eu(II) sites emissions of β-SSO is ~480nm and ~540nm respectively.[33] The DPWs of the Eu(I) and Eu(II) sites emissions of ordered α'-SSO is ~490nm and ~560nm respectively.[34] As shown in Fig. 7, compared with the β-SSO: Eu^{2+}, after N^{3-} substituting for O^{2-}, under 375nm excitation, the DPWs of Eu(I) (~465nm) and Eu(II) (~536nm) sites emissions appeared a slight red-shift. Under 460nm excitation, the emission peak of Eu(I) site almost disappeared and the emission peak of the Eu(II) sites appeared an obvious red-shift, which was changed from 543nm to 612nm. However, the PL spectra of β-SSON: Eu^{2+} appeared another impurity emission peak at 537nm, which should be attributable to the emission of β-SSO: Eu^{2+} phosphor.[29, 33] In addition, Fig. 6 shows a weaker peak of Sr/Eu–N bond (1439 cm^{-1}) also indicated that the $Sr_{1.98-x}Ba_xSi(O,N)_4$ (x=0) sample of our experiments was the mixed phase of β-$Sr_{1.98}Si(O,N)_4$ and β-$Sr_{1.98}SiO_4$ phase. However, due to the similar electronic configuration between O and N, the β-SSO and β-SSON phases couldn't be distinguished effectively by X-ray diffraction analysis.[28] Besides, the introduction of N^{3-} would result in the decrease of PL intensity, as shown in the PL and PLE spectra in Fig. 7.

The partial incorporation of N^{3-} ions caused a strong crystal field splitting and gave rise to a nephelauxetic effect.[21] The strong crystal field could be ascribed to the stronger covalent properties of Eu-O/N bond. The nephelauxetic effect was related to appropriate centroid shift in the RE cation d-orbitals and can be attributed to the covalency between the RE cation and the surrounding anions, as well as their polarizability (the performance of the deformation).[35, 36]

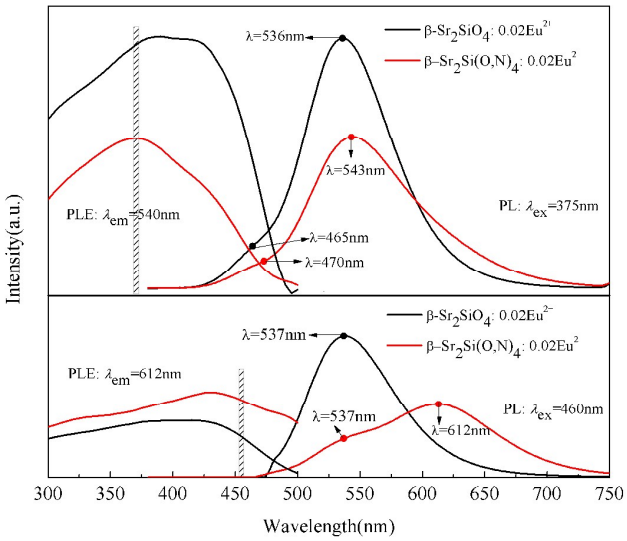

Fig. 7 PLE and PL spectra comparison of β-SSO: 0.02Eu^{2+} and β-$Sr_{1.98}Si(O,N)_4$: 0.02Eu^{2+}.

The 5d centroid shift for Eu^{2+} can be expressed by the following equation:[2]

$$\varepsilon_c = A\sum_{i=1}^{N}\frac{a_{SP}^{i}}{(R_i - 0.6\Delta R)^6} \qquad (1)$$

where A is a constant, α_{SP}^{i} is the spectroscopic polarizability of anion i, R_i is the distance between Eu^{2+} and anion i in the undistorted lattice, and ΔR is the difference between the radii of Eu^{2+} and Sr^{2+} in different sites. The polarizability α_{SP}^{i} of N is larger than that of O because N has the lower electronegativity (3.04) and the weaker ability of electronic attraction. So the partial incorporation of N^{3-} ions could give rise to a centroid shift (so called nephelauxetic effect). These factors induced the lowest 5d

CrystEngComm Accepted Manuscript

This journal is © The Royal Society of Chemistry 20xx

excitation level of the Eu^{2+} ions shifted toward the ground level at the Eu(II) site. Hence, the 5d energy levels of Eu^{2+} ions is declined, which led to long wavelength emission (~610nm) suitable for low energy blue LED excitation rather than n-UV excitation. And there appeared a red-shift in β-SSO: Eu^{2+} after N substituting for O. Besides, the Eu(I)(CN=10) sites was not significantly affected by nitridation. This was because Eu(II) (CN=9) sites had smaller coordination number (CN) and the bond length of Eu(II)-N was shorter than that of Eu(I)–N. Unfortunately, as shown in Fig. 3 (b), with the introduction of N^{3-} ions, an asymmetric Si-NO_3 tetrahedron was observed in local scale, which undermined the crystal symmetry. At the same time, the degree of crystallinity for β-SSON: Eu^{2+} became worse due to the increased proportion of Si-N and (Sr/Eu)–N bonds, as shown in Fig. 1. Hence, the PL intensity of β-SSO: Eu^{2+} obviously decreased with the N entered into the lattice, as shown in Fig. 7.

Fig. 8 shows the photoluminescence (PL) spectra of $Sr_{1.98-x}Ba_xSi(O,N)_4$: $0.02Eu^{2+}$ ($0 \le x \le 0.5$) with varying Ba content under 375nm and 460 nm excitation and the corresponding photoluminescence excitation (PLE) spectra. On the basis of the occupation of sites by Eu^{2+} in domains of different coordination environment, a color point tuning in single-phase host can be realized, as shown in Fig. 8. In order to ensure the precision of the PL intensity and emission wavelengths, the tests of the PL and PLE spectra were ran 5 times. It shows that the emission wavelengths hardly changed while the PL intensity changed slightly, as shown in the inset of Fig. 8. Due to the complexity of the PL spectra, the discussion would be divided into two parts: (1) the PL spectra with the increase of Ba^{2+} content from 0 to 0.1; (2) the PL spectra with the increase of Ba^{2+} content from 0.1 to 0.5.

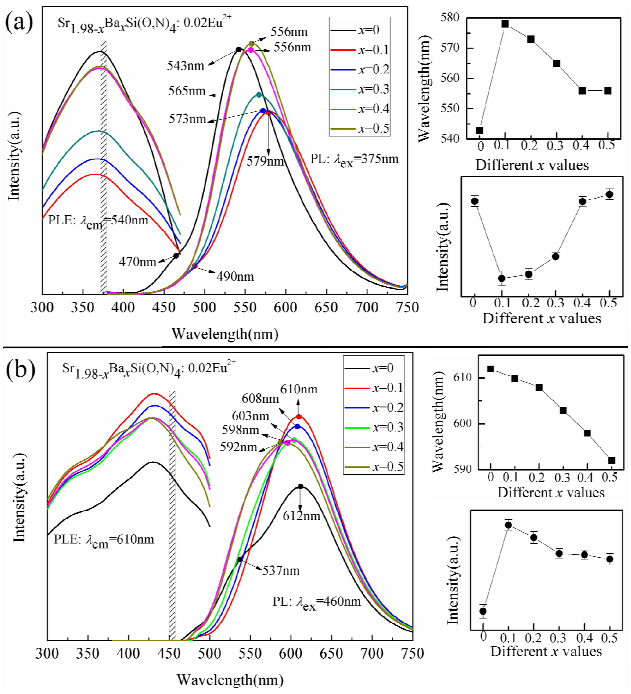

Fig. 8 PLE and PL spectra of $Sr_{1.98-x}Ba_xSi(O,N)_4$: $0.02Eu^{2+}$ ($0 \le x \le 0.5$) with varying Ba content: (a) 375nm excitation and (b) 460nm excitation.

With the substitution of 0.1 mol Ba^{2+} for Sr^{2+}, under 375nm excitation, the DPWs of the Eu(I) sites changed from 470nm to 490nm and that of the Eu(II) sites changed from 543nm to 579nm. Both the PL intensity of Eu(I) and Eu(II) sites declined. Under 460nm excitation, the DPWs of the Eu(II) sites of β-SSO: Eu^{2+} (537nm) disappeared and that of β-SSON: Eu^{2+} (612nm) was hardly changed. Besides, the PL intensity of 612nm was significantly improved. The change of emission peak sites was due to the phase transformation from β phase to α'-SBSON phase as shown in Fig. 1 and Fig.2. The decrease of PL intensity of Eu(I) and Eu(II) sites unpon 375 nm excitation was because the phase transformation from β to α' led to a red-shift. A short wavelength ultraviolet light excited to induce a longer emission wavelength, which need to larger stokes shift and energy. The significant improvement of the PL intensity of red emission at Eu(II) sites under 460 nm excitation was because the proper Ba^{2+} content (x=0.1) could obtain a pure α' phase (as shown in Fig. 1 and Fig. 2). Whereas the sample of undoped Ba^{2+} was the mixture phase of β-SSO: Eu^{2+} and β-SSON: Eu^{2+}.

With the increase of Ba^{2+} content from 0.1 to 0.5, unpon 375nm excitation, the DPWs of the Eu(I) and Eu(II) sites emissions appeared a obvious blue-shift, the PL intensity of Eu(I) and Eu(II) sites gradually raised. Unpon 460nm excitation, the DPWs of Eu(II) sites emissions had hardly changed with a small amount replacement of Ba^{2+} ($0.1 \le x \le 0.2$) and appeared a obvious blue-shift with a large amount replacement of Ba^{2+} ($0.3 \le x \le 0.5$). The PL intensity of Eu(II) sites gradually declined with the increase of Ba content from 0.1 to 0.5. In fact, with the increase of Ba^{2+} content from 0.1 to 0.5, the PL intensity of SBSON: Eu^{2+} gradually increased upon the 375 nm excitation while gradually decreased upon 460 nm excitation. This opposite phenomenon is difficult to be ascribed to the measuring error or external environment (such as temperature, impurity phase, atmosphere and so on). Base on this point, this phenomenon only can be caused by the incorporation of Ba^{2+}. Generally, the ultraviolet light excitation (λ_{ex}=375nm) made short wavelength emission more efficient, whereas the blue light excitation (λ_{ex}=460nm) made long wavelength emission more efficient. This could be ascribed to the short wavelength emission at higher energy site and long wavelength emission at lower energy site.[37] As shown in Fig. 8, the PLE spectra indicated that the ultraviolet light excitation (λ_{ex} = 350-400 nm) was more beneficial to short wavelength emission (540nm), whereas the blue light excitation (λ_{ex} = 420-460 nm) was more beneficial to long wavelength emission (610nm). The further interpretations of these phenomena of Fig. 8 will be discussed in detail in the following paragraphs.

CrystEngComm Accepted Manuscript

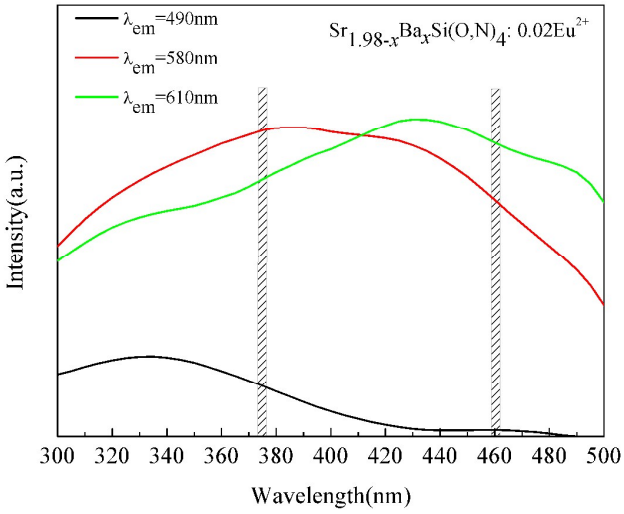

Fig. 9 PLE spectra of $Sr_{1.88}Ba_{0.1}Si(O,N)_4$: 0.02$Eu^{2+}$ corresponded to 490nm, 580nm, 610nm emission, respectively.

Fig. 9 shows the excitation spectra of the α'-$Sr_{1.88}Ba_{0.1}Si(O,N)_4$: 0.02$Eu^{2+}$ monitored at 490nm, 580nm, 610nm emission peaks. As shown in Fig. 9, the emission of Eu(I) (490nm) site only could be excited by UV light. The blue light (λ_{em}=460nm) excitation led to efficient longer red light emission (610nm) of Eu(II) site than UV-light excitation. The UV excitation (λ_{ex}=375nm) is weighted against the red emission (610nm) of Eu(II) site but make for yellow emission (580nm) of Eu(II) site. The $Sr_{1.88}Ba_{0.1}Si(O,N)_4$: 0.02$Eu^{2+}$ can realize an intense red emission at ~610nm under 400–500 nm excitation.

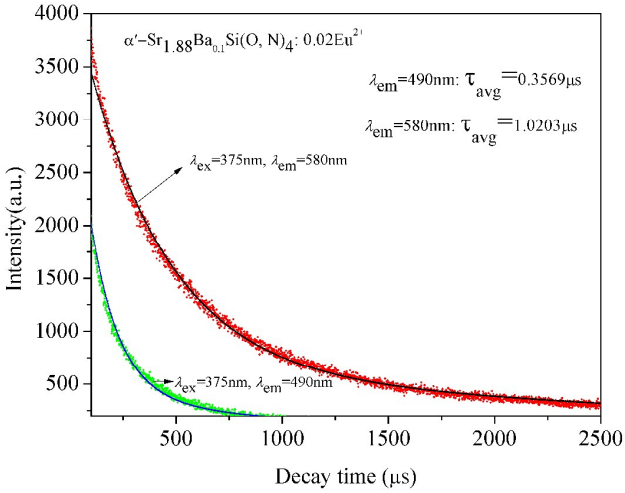

Fig. 10 PL decay curves of $Sr_{1.88}Ba_{0.1}Si(O,N)_4$: 0.02$Eu^{2+}$ (λ_{ex}=375nm, λ_{em}=490nm; λ_{ex}=375nm, λ_{em}=580nm).

The PL decay curves of the Eu^{2+} ions in $Sr_{1.88}Ba_{0.1}Si(O,N)_4$: 0.02$Eu^{2+}$ phosphors were obtained with excitation at 375 nm, monitored at 490 nm and 580 nm respectively, as shown in Fig. 10. The varying decay curves of the Eu^{2+} ions can be fitted well to a typical double-exponential decay curve using the following equation: [38-40]

$$I(t) = A_1 \exp(\frac{-t}{\tau_1}) + A_2 \exp(\frac{-t}{\tau_2}) \quad (2)$$

where *I* represents the luminescent intensity, *A1* and *A2* are constants, *t* is time, τ_1 and τ_2 are the decay times for the exponential components. The average decay time (τ*) can be calculated using the following equation: [41, 42]

$$\tau = \frac{\int_0^\infty I(t)tdt}{\int_0^\infty I(t)dt} \quad (3)$$

where *I(t)* is the intensity at time *t*. The average lifetime of the Eu^{2+} ions is determined to be 0.3569 μs and 1.0203 μs for α'-SBSON: 0.02Eu^{2+} with the monitored wavelength at 490 nm and 580 nm respectively. In general, the emission decay times are similar when active ions occupy the same site.[43] Fig. 8(a) presents the emission decay of Eu^{2+}: at 490 nm in Eu(I) site and 580 nm in Eu(II) site upon 375nm excitation. It is clear that the lifetime of Eu^{2+} in two sites above is different, which can demonstrate the existence of two sites in α'-SBSON: 0.02Eu^{2+}.[43]

Fig. 11 shows the diffuse reflection spectra of β-$Sr_{1.98}SiO_4$: 0.02Eu^{2+} and $Sr_{1.98-x}Ba_xSi(O,N)_4$: 0.02Eu^{2+} (*x*= 0, 0.1 and 0.5). Compared with the β-$Sr_{1.98}SiO_4$: 0.02Eu^{2+}, the absorption band of $Sr_{1.98}Si(O,N)_4$: 0.02Eu^{2+} appeared a remarkable red-shift, as shown in the right shaded area of Fig. 11. It could be ascribed to the decline of 5d level of Eu^{2+} and larger crystal field splitting depending on the N^{3-} substitution. With the increase of Ba^{2+} content from 0 to 0.1, the absorption in 400-500 nm increased significantly, while the absorption in 300-400 nm increased slightly. This was because of the phase transformation from β - SSON to α' - SBSON phase. With the increase of Ba^{2+} content from 0.1 to 0.5, the absorption in 400-500 nm hardly changed, while the absorption in 300-400 nm increased significantly. It could be attributed to the enhanced absorption of host lattice due to the large amount of Ba^{2+} introduction.

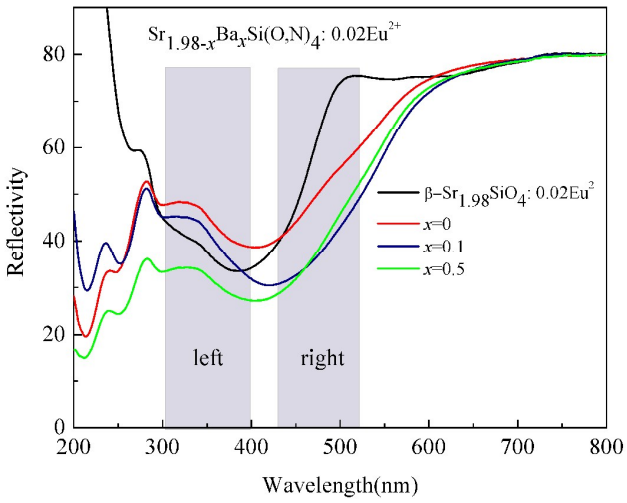

Fig. 11 Diffuse reflection spectra of β-Sr_2SiO_4: 0.02Eu^{2+} and $Sr_{1.98-x}Ba_xSi(O,N)_4$: 0.02Eu^{2+} (*x* = 0, 0.1 and 0.5).

CrystEngComm Accepted Manuscript

This journal is © The Royal Society of Chemistry 20xx

Fig. 12 shows the diffuse reflection spectra (DRS) of $Sr_2Si(O,N)_4$, $Sr_{1.5}Ba_{0.5}Si(O,N)_4$ host materials and the Eu^{2+} doped $Sr_{1.48}Ba_{0.5}Si(O,N)_4$: $0.02Eu^{2+}$ phosphor. As shown in the shaded area of Fig. 12, the substitution of Ba^{2+} led to an obvious red-shift of the absorption band. The absorption band of $Sr_{1.5}Ba_{0.5}Si(O,N)_4$ was located in ultraviolet region, which was range from ~265nm (4.7eV) to ~341nm (3.6eV). As a contrast, the doping of Eu^{2+} significantly enhanced the absorption from the ultraviolet to blue light region which was caused by the typical $4f^7$-$4f^65d^1$ transition.[26, 44] These results indicated that Ba^{2+} only could enhance the absorption in the ultraviolet region.

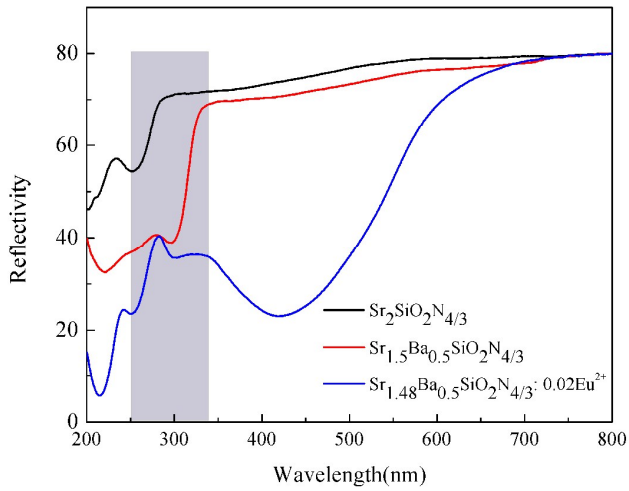

Fig. 12 Diffuse reflection spectra of $Sr_2Si(O,N)_4$, $Sr_{1.5}Ba_{0.5}Si(O,N)_4$ and $Sr_{1.48}Ba_{0.5}Si(O,N)_4$: Eu^{2+}.

Fig. 13 shows the energy level diagram of Ba^{2+} and Eu^{2+} in SBSON: $0.02Eu^{2+}$. According to the diffuse reflection spectra in Fig. 12, the 5d orbital of Ba^{2+} was located on a higher energy site (~3.6-4.7 eV), which was close to the higher energy level of 5d orbital of Eu^{2+} (~2.4-3.75 eV),[45] as shown in Fig. 13. Hence, the 5d orbital of Ba^{2+} coupled with the 5d orbital of Eu^{2+} on the higher energy level position in the host crystal.[46] It was equivalent to that the density of states of higher 5d energy level was enhanced. Therefore, as shown in Fig. 8, with the increase of Ba^{2+} content from 0.1 to 0.5, the PL intensity of yellow-green emission gradually increased under the 375 nm excitation. On the other hand, the PL intensity of red-orange emission gradually decreased under the 460 nm excitation. It could be ascribed to the fact that blue-shift weakened the PL intensity of red light emission depend on the smaller stokes shift and the introduction of Ba^{2+} didn't make contribution to blue light excitation due to the 5d orbital of Ba^{2+} wasn't located on a lower energy site.

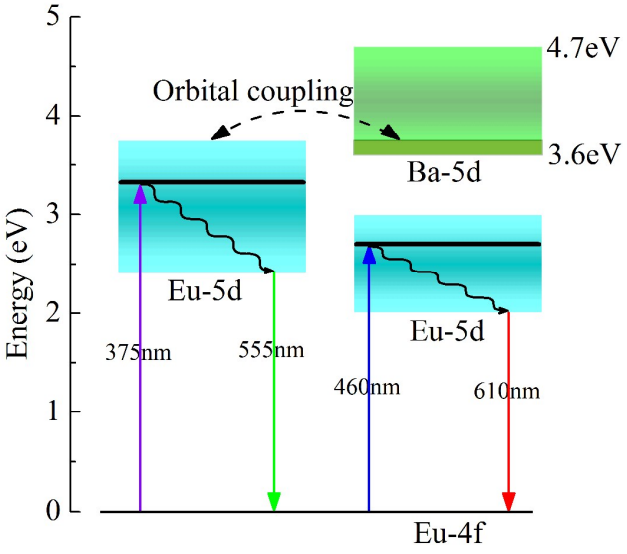

Fig. 13 The energy level diagram of Ba^{2+} and Eu^{2+} in SBSON: $0.02Eu^{2+}$.

As shown in Fig. 8, whether the SBSON: Eu^{2+} was excited by UV light or blue light, a large amount replacement of Ba^{2+} ($0.3 \le x \le 0.5$) could lead to an obvious blue-shift phenomenon. Because the similar ionic radii between Sr^{2+} (1.31 Å, 9CN; 1.36 Å, 10CN) and Eu^{2+} (1.30 Å, 9CN; 1.35 Å, 10CN), and the Ba^{2+} (1.49 Å, 9CN, 1.52 Å, 10CN) had larger ionic radii, the Eu^{2+} would preferentially occupy Sr^{2+} sites in SBSON.[37] Thus, a small amount replacement of Ba^{2+} ($0.1 \le x \le 0.2$) hardly led to an obvious blue-shift phenomenon. The Eu^{2+} would gradually occupy Ba^{2+} sites in SBSON host when a large amount of Ba^{2+} ($0.3 \le x \le 0.5$) substituted for Sr^{2+}, which led to a obvious blue-shift.[37] The blue-shift was related to the influence of Ba-content on the crystal-field strength and the covalence state. The crystal field splitting (Dq) can be determined by the following equation:[47, 48]

$$Dq = \frac{1}{6} Ze^2 \frac{r^4}{R^5} \quad (4)$$

where Dq is a measure of the energy level separation, Z is the anion charge, e is the electron charge, r is the radius of the d wavefunction, and R is the bond length. When larger Ba^{2+} ions partially substituted for smaller Sr^{2+} ions in the host lattice, bond length increased, which led to the lattice constants expansion of α'-SSON, as shown in Table 4. It caused weakening of crystal field strength.[49, 50] In addition, the electronegativity of Ba^{2+} (0.89) is lower than that of Sr^{2+} (0.95). With the increase of Ba^{2+} content, the difference of electronegativity between cation and anion (electronegativity: N is 3.04, O is 3.44) would increase, which result in the covalency of the host lattice decreased. Thus, the crystal field strength became weak, which lead to an obvious blue-shift in the SBSON: Eu^{2+}. On the other hand, the alkaline earth ions form chains along the c axis in orthorhombic form of Sr_2SiO_4.[51] The Eu^{2+} randomly occupied Sr1 and Sr2 sites and form two luminescence centers Eu(I) and Eu(II) respectively. The positive charges can orient one d-orbital preferentially. As the length of the

CrystEngComm Accepted Manuscript

c axis increases, the effect of preferential orientation of a d-orbital in the chain direction decreases so that the Eu^{2+} emission shifts to shorter wavelength.[52,53] Therefore, a blue-shift of the 5d-4f transition of Eu^{2+} should occur.

Besides, according the eqn(4) and Fig.3 (b) and (c), compared with the α'-SSO, the N^{3-} doping lead to the shorter Sr2-O1 (3.105 Å *vs*. 2.881 Å, 3.105 Å vs 2.744 Å) bond length. Similarly with the Si-$(N/O)_4$ tetrahedron, the Sr2-O1 bond might be squeezed by the longer Sr1-N bond (2.879 Å, 2.972 Å) because the N^{3-} ions was simultaneously connected to Sr1 and Sr2 sites . The *R* value of Eu(II) sites ligand get smaller. Therefore, the crystal-field strength is more influential on emission of the 9-oxygen coordinated Eu(II) sites than that of Eu(I) sites. [21]

For application in high power LEDs, the thermal stability of phosphors is one of the important issues to be considered. The temperature quenching performances of β-SSO: Eu^{2+}, β-SSON: Eu^{2+} and α'-SBSON: Eu^{2+} phosphors are shown in Fig. 14. As shown in Fig. 14, it could be observed that the thermal stability of α'-SBSON: Eu^{2+} is superior to that of β-SSO: Eu^{2+} and β-SSON: Eu^{2+}. In fact, according the previous discussion, the pure β-SSON: Eu^{2+} phase wasn't obtained in our experiments and it had some β-SSO: Eu^{2+} impurity phases. This thermal phenomenon could be ascribed to the improvement of stability of α' phase depending on the Ba^{2+}. The introduction of Ba^{2+} led to a greater rigid lattice, which in turn results in the highest luminescence efficiency for intermediate compositions at elevated temperatures. [1] As the Ba^{2+} substitution for the Sr^{2+} site would cause a longer and looser Ba-O compared with the Sr-O, Ba^{2+} ions should preferentially coordinate the N^{3-} and O^{2-} in SBSON: Eu^{2+}. The partial Eu^{2+} substituted for Ba^{2+}, which led to the result that above-average numbers of N^{3-} and O^{2-} was clustered surrounding Eu^{2+}. Therefore, the binding strength of Eu-O/N is slightly improved as partial Ba^{2+} replacing Sr^{2+}, resulting in a large force constant and a low thermal quenching.[54] Besides, the introduction of N could enhance the thermal stability. Compared with O, N have less lone pair electron and could form more chemical bond, which could lead to the result that more complex structure and the better thermal stability.

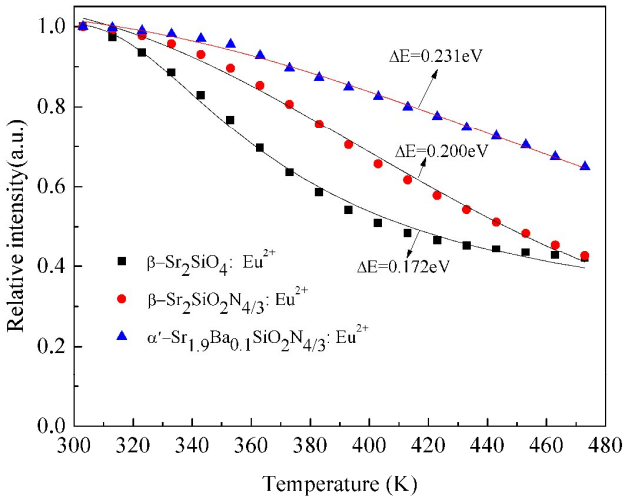

Fig. 14 Temperature quenching performances of β-SSO: Eu^{2+}, β-SSON: Eu^{2+} and α'-SBSON: Eu^{2+} phosphors.

To determine the activation energy for thermal quenching, the Arrhenius equation was fitted to the thermal quenching data.[47, 55, 56]

$$I(T) = \frac{I_0}{1 + c\exp(\frac{-E}{kT})} \quad (5)$$

Where I_0 is the initial intensity, $I(T)$ is the intensity at a given temperature *T*, *c* is a constant, *E* is the activation energy for thermal quenching, and *k* is Boltzmann's constant. The curves in Fig. 14 were obtained by fitting according to the equation 5. The fitting results give a comparable activation energy *E* of 0.231 eV for α'-SBSON: Eu^{2+}, 0.200 eV for β-SSON: Eu^{2+} and 0.172 eV for β-SSO: Eu^{2+}. By increasing the temperature up to 150 ℃ at which the white LEDs usually work, the emission intensity of the α'-SBSON: Eu^{2+} phosphor remained at 78% of that measured at room temperature.

4 Conclusions

The $Sr_{1.98-x}Ba_xSi(O,N)_4$: $0.02Eu^{2+}$ ($0 \le x \le 0.5$) phosphors were prepared by conventional solid state reaction method. The Sr-N and Si-N bond were confirmed by FT-IR spectra and crystal structure. Specially, compared with the Sr_2SiO_4: Eu^{2+}, the XRD refinement results indicated that N^{3-} would substitute for $O2^{2-}$ site and form Si-NO3 tetrahedrons during the process of forming SSON: Eu^{2+} substitutional solid solution. The SSON: Eu^{2+} phosphors exhibited broad excitation spectra and a strong red emission ~ 610nm at Eu(II) sites. Ba^{2+} doping could achieve the phase transformation from the β phase to α'-SBSON phase. The lattice constants were expanded with the introduction of Ba^{2+}, which could be attributed to the longer bond length of Ba–O. On the premise that the red emission peaks were not changed under 460nm excitation, the substitution of 0.1 mol Ba^{2+} ions could enhance the PL intensity of SSON: Eu^{2+}. Whereas the substitution with 0.5 mol Ba^{2+} ions could enhance the PL intensity of green light emission in SSON: Eu^{2+}. Both Ba^{2+} and N^{3-} doping could improve the thermal stability of Sr_2SiO_4: Eu^{2+} phosphor. For the adjustable emission properties from green to red and the enhanced PL intensity by Ba^{2+} doping in the SSON: Eu^{2+} phosphor, it could be a good candidate for use in white light emitting diodes.

Acknowledgements

This work was financially supported by the National Natural Science Foundation of China (Grant nos. 51272243 and 61405185), the Zhejiang Provincial Natural Science Foundation of China (LY14E020008 and LZ14F050001).

Notes and references

CrystEngComm Accepted Manuscript

This journal is © The Royal Society of Chemistry 20xx

1 K. A. Denault, J. Brgoch, M.W. Gaultois, A. Mikhailovsky, R. Petry, H. Winkler, S. P. D. Baars and R. Seshadri, *Chem. Mater.*, 2014, **26**, 2275.
2 S. Miao, Z. Xia, M. S. Molokeev, M. Chen, J. Zhang, Q. Liu, *J. Mater. Chem. C*, 2015, **3**, 4616.
3 S. Miao, Z. Xia, J. Zhang, and Q. Liu, *Inorg. Chem.*, 2014, **53**, 10386.
4 W. Lv, M. Jiao, Q. Zhao, B. Shao, W. Lü, and H. You, *Inorg. Chem.*, 2014, **53**, 11007.
5 L. Chen, A. Luo, Y. Zhang, F. Liu, Y. Jiang, Q. Xu, X. Chen, Q. Hu, S. Chen, K. Chen, and H. Kuo. *ACS Comb. Sci.*, 2012, **14**, 636.
6 Z. Xia, S. Miao, M. Chen, M. S. Molokeev, and Q. Liu, *Inorg. Chem.*, 2015, **54**, 7684.
7 W. Ji, M. Lee, L. Hao, X. Xu, S. Agathopoulos, D. Zheng and C. Fang, *Inorg. Chem.*, 2015, **54**, 1556.
8 B. G. Hyde, J. R. Sellar and L. Stenberg, *Acta Crystallogr., Sect.B: Struct. Sci.B*, 1986, **42**, 423.
9 J.K. Park, M.A. Lim, C.H. Kim, H.D. Park, J.T. Park and S.Y. Choi, *Appl. Phys. Lett.*, 2003, **82**, 683.
10 L.C.Ju, C. Cai, Q.-Q. Zhu, J.Y.Tang, L.Y.Hao and X. Xu, *J.Mater. Sci.: Mater. Electron.*, 2013, **24**, 4516.
11 J.K. Park, C.H. Kim, S.H. Park, H.D. Park and S.Y. Choi, *Appl. Phys. Lett.* , 2004, **84**, 1647.
12 M. Catti, G. Gazzoni and G. Ivaldi, *Acta Crystallogr., Sect. C:Cryst. Struct.Commun.*, 1983, **39**, 29.
13 M. Catti,G. Gazzoni and G. Ivaldi, *Acta Crystallogr., Sect. B Struct.Commun.*, 1983. **39**, 674.
14 M. Catti,G. Gazzoni and G. Ivaldi, *Acta Crystallogr., Sect. B Struct.Commun.*, 1983. **39**, 679.
15 J.S. Kim, P.E. Jeon, J.C. Choi and H.L. Park, *Solid State Commun.*, 2005, **133**, 187.
16 J. H. Lee and Y. J. Kim, *Mater. Sci. Eng., B*, 2008, **146**, 99-102.
17 J. K. Han, M. E. Hannah and A. Piquette, *J. Lumin.*, 2012, **132**, 106.
18 K.S. Sohn, J. H Kwak, Y.S Jung, H. Yan and M J. Reece, *J. electrochem. Soc.*, 2008, **155**, J58.
19 Z. Zhao, Z. Yang, Y. Shi, C. Wang, B. Liu, G. Zhu and Y. Wang, *J. Mater. Chem. C*, 2013, **1**, 1407.
20 S. J. Lee, S. H. Hong and Y. J. Kim, *J. Electrochem. Soc.*, 2012, **159**, J163.
21 J. Park, S. J. Lee and Y. J. Kim, *Cryst. Growth Des.*, 2013, **13**, 5204.
22 J. Ju, L. Cheng, X. Xu, L.Y. Hao, Y. Lin and M.-H Lee, *J. Mater. Chem. C*, 2015, **3**, 1567.
23 X. Li, Y. Hua, H. Ma, D. Deng, G. Jia and S. Xu, *RSC Adv.*, 2015, **5**, 62659.
24 A. Nag and T. R. N. Kutty, *J. Mater. Chem.*, 2004, **14**, 1598.
25 W. J. Xie, Y.C. Wang, X. Xu and C.S. Chen, Chem. Lett., 2008, **37**, 498.
26 D. Dutczak, T. Jüstel, C. Ronda and A. Meijerink, *Phys. Chem. Chem. Phys.*, 2015,**17**, 15236.
27 K. J. D. MacKenzie, G. J. Gainsford and M. J. Ryan, *Journal of the Europium Ceramic Society*, 1996, **16**, 553.
28 X. M. Wang, C. H. Wang, X. J. Kuang, R. Q. Zou, Y. X. Wang and X. P. Jing, *Inorg. Chem.*, 2012, **51**, 3540.
29 O. Oeckler, F. Stadler, T. Rosenthal and W. Schnick, *Solid State Sci.*, 2007, **9**, 205.
30 R. W. G. Syme, D. J. Lockwood and H. J. J. Kerr, *Phys. C, Vol.*, 1977, **10**, 335.
31 J. Etchepare, *Spectrochim, Acta*, 1970, **26A**, 2147.
32 P. McMillan, *Am. Mineral*, 1984, **69**, 622.
33 Lakshminarasimhan and U.V. Varadaraju, *J. Electrochem. Soc.*, 2005, **152**, H152.
34 S.H.M. Poort, W. Janssen and G. Blasse, *J. Alloys Compd.*, 1997, **260**, 93.
35 T. M. Tolhurst , T. D. Boyko , P. Pust , N. W. Johnson , W. Schnick and A. Moewes, *Adv. Optical Mater.*, 2014, DOI: 10.1002/adom.201400558.
36 P. Dorenbos, *Phys. Rev. B*, 2001, **64**, 125117.
37 G. Li, C. C. Lin, W-T. Chen, M. S. Molokeev,V. V. Atuchin, C-Y. Chiang, W. Zhou, C-W. Wang, W-H. Li, H-S. Sheu, T-S. Chan, C. Ma and R-S. Liu, *Chem. Mater.*, 2014, **26**, 2991.
38 J. Huang, X. Hu, J. Shen, D. Wu, C. Yin, R. Xiang, C. Yang, X. Liang, and W. Xiang, *CrystEngComm*, 2015, **17**, 7079-7085.
39 Q. Wu, Z. Yang, Z. Zhao, M. Que, X. Wang and Y. Wang, *J. Mater. Chem. C*, 2014, **2**, 4967.
40 M. Yu, J. Lin and J. Fang, *Chem. Mater.*, 2005, **17**, 1783–1791.
41 Z. Xia, and R.S. Liu, *J. Phys. Chem. C*, 2012, **116**, 15604−15609.
42 G. Zhu, Y. Shi, M. Mikami, Y. Shimomura and Y. Wang, *CrystEngComm*, 2014, **16**, 6089.
43 Y. Chen, Y. Li, J. Wang, M. Wu, and C. Wang, *J. Phys. Chem. C*, 2014, **118**, 12494.
44 Y. Jia, H. Qiao, Y. Zheng, N. G and H. You, *Phys. Chem. Chem. Phys.*, 2012, **14**, 3537.
45 J. Y. Tang, J. H. Chen, L.Y. Hao, X. Xu, W. J. Xie, and Q. X. Li, *J. Lumin.*, 2011, **131**, 1101.
46 J.G. Sole, L.E. Bausa and D. Jaque, An Introduction to the Optical Spectroscopy of Inorganic Solid, *John Wiley & Sons, Ltd.*, New York, 2005.
47 M. Que, Z. Ci, Y. Wang, G. Zhu, S. Xin, Y. Shi and Q. Wang, *CrystEngComm*, 2013, **15**, 6389.
48 P. D. Rack and P. H. Holloway, *Mater. Sci. Eng.*, 1998, **21**, 171.
49 G. Blasse and B.C. Grabmaier, Luminescent Material, *Springer*, Berlin, 1994.
50 S.H.M. Poort and G. Blasse, *J. Lumin.*, 1997, **247**, 72.
51 S.H.M. Poort, W. Janssen and G. Blasse, *J.Alloys Compd.*, 1997, **93**, 260.
52 J. K. Park, K. J. Choi, S. H. Park, C. H. Kim and H. K. Kim, *J. Electrochem. Soc.*, 2005, **152**, H121.
53 S. H. M. Poort, J. W. H. van Krevel, R. Stomphorst, A. P. Vink, and G. Blasse, *J.Alloys Compd.*, 1996, **75**, 241.
54 L. Chen, W. Zhuang, R. Liu, Y. Liu, Y. Hu, X. Ma, X. Zhou and W. Gao, *CrystEngComm*, 2015, **17**, 3687-3694.
55 R-J Xie, N. Hirosaki, N. Kimura, K. Sakuma and Mamoru Mitomo, *Appl. Phys. Lett.*, 2007, **90**, 191101.
56 S. Bhushan and M. V. Chukichev, *J. Mater. Sci. Lett.*, 1988, **9**, 319.

CrystEngComm Accepted Manuscript

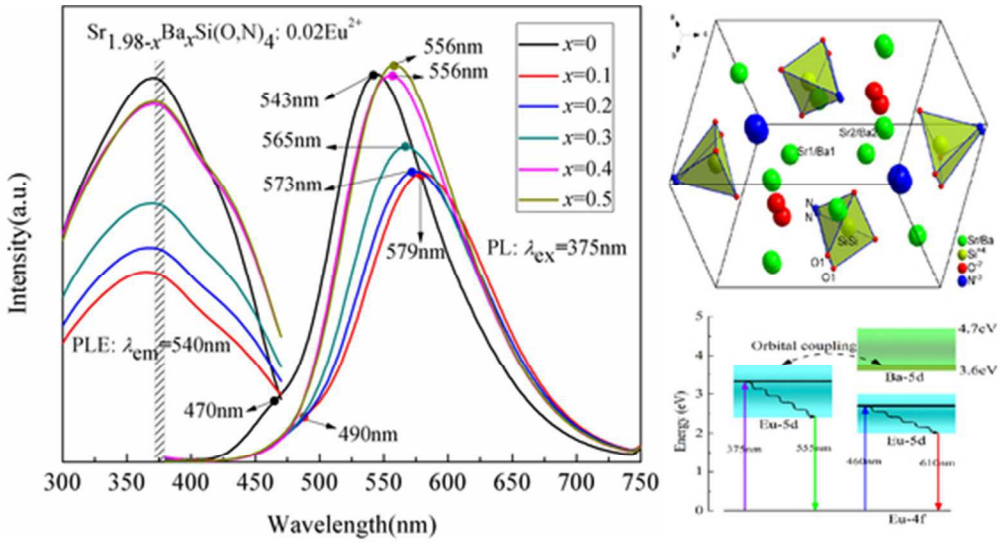

graphical abstract
48x26mm (300 x 300 DPI)

CrystEngComm Accepted Manuscript